PHYSICAL REVIEW B **78**, 214424 (2008)

High magnetic moments and anisotropies for Fe_xCo_{1-x} monolayers on Pt(111)

G. Moulas,[1] A. Lehnert,[1] S. Rusponi,[1] J. Zabloudil,[2] C. Etz,[3] S. Ouazi,[1] M. Etzkorn,[1] P. Bencok,[4] P. Gambardella,[5] P. Weinberger,[3] and H. Brune[1]

[1]*Institute of the Physics of Nanostructures, Ecole Polytechnique Fédérale de Lausanne (EPFL), CH-1015 Lausanne, Switzerland*

[2]*Institut für Physikalische Chemie, University of Vienna, Sensengasse 8/7, A-1090 Vienna, Austria*

[3]*Center for Computational Materials Science, Vienna University of Technology, Getreidemarkt 9/134, A-1060 Vienna, Austria*

[4]*European Synchrotron Radiation Facility, Boîte Postale 200, F-38043 Grenoble, France*

[5]*Centre d'Investigacions en Nanociència i Nanotecnologia (ICN-CSIC), UAB Campus, E-08193 Bellaterra, Spain and Institució Catalana de Recerca i Estudis Avançats (ICREA), E-08100 Barcelona, Spain*

(Received 31 July 2008; published 17 December 2008)

The magnetism of 1-ML-thick films of Fe_xCo_{1-x} on Pt(111) was investigated both experimentally, by x-ray magnetic circular dichroism and magneto-optical Kerr effect measurements, and theoretically, by first-principles electronic structure calculations, as a function of the film chemical composition. The calculated Fe and Co spin moments are only weakly dependent on the composition and close to $3\mu_B$/atom and $2\mu_B$/atom, respectively. This trend is also seen in the experimental data, except for pure Fe, where an effective spin moment of only $S_{\text{eff}}=(1.2\pm0.2)\mu_B$/atom was measured. On the other hand, both the orbital moment and the magnetic anisotropy energy show a strong composition dependence with maxima close to the $Fe_{0.5}Co_{0.5}$ stoichiometry. The experiment, in agreement with theory, gives a maximum magnetic anisotropy energy of 0.5 meV/atom, which is more than 2 orders of magnitude larger than the value observed in bulk bcc FeCo and close to that observed for the $L1_0$ phase of FePt. The calculations clearly demonstrate that this composition dependence is the result of a fine tuning in the occupation number of the $d_{x^2-y^2}$ and d_{xy} orbitals due to the Fe-Co electronic hybridization.

DOI: 10.1103/PhysRevB.78.214424 PACS number(s): 75.70.Ak, 75.30.Gw, 73.20.At

I. INTRODUCTION

Exploring the ultimate density limits of magnetic information storage requires elaborate tuning of several magnetic properties, such as the easy magnetization axis, the magnetic anisotropy energy (MAE) K, and the saturation magnetization (M_S) of the recording medium.[1] In order to inhibit thermally activated magnetization reversal the MAE has to be 1.2 eV/bit. Reducing the bit size therefore requires higher MAE per atom. At the same time, the magnetization density of the recording medium must increase in order to stay with technologically available write fields. In order to reduce dipolar magnetic interactions between adjacent bits the easy axis has to be perpendicular to the plane, and finally narrow switching and stray field distributions are required.

Extensive theoretical and experimental efforts have been devoted to develop new materials that meet these requirements. Examples are patterned media, exchanged-biased multilayers, and self-assembled monodisperse and equidistant nanoparticles. Bimetallic alloys represent a viable route to tune both M_S and the MAE, as these quantities are strongly influenced by compositional effects and lattice distortions. While the MAE of ferromagnetic transition metals in their cubic structures is on the order of a few tens of μeV/atom, structurally distorted alloys, such as FePt in the $L1_0$ phase[2–4] or bct-FeCo,[5–7] may have MAE values close to 1 meV/atom. Moreover, the total magnetic moment can be tuned by choosing the two elements of the alloy. FePt and FeCo are good examples of alloys with comparable MAE but with, respectively, lower and higher magnetic moments with respect to Fe and Co bulk values.

As the typical size of nanoparticles and the thickness of thin films approach a few atomic lattice distances, electronic interactions between the magnetic medium and the supporting substrate play an increasingly important role and lead to new properties opening up a new degree of freedom. The effect of electronic hybridization with the substrate is well exemplified by the magnetic behavior observed for surface-adsorbed individual atoms. Giant magnetic anisotropies have been found for single Co atoms on Pt(111),[8] a 5d transition metal, while vanishing MAE values have been observed for single Co atoms when deposited on alkali metals where only 3d-sp hybridization is possible.[9] In addition to electronic change via hybridization, in thin films the lattice mismatch between film and substrate can induce modifications of the crystallographic translational symmetry, which can result in additional modifications of the magnetic properties.[10]

Here we report on the magnetic properties of 1 ML (monolayer) (1 ML is defined as 1 film atom per substrate atom) thick films of Fe_xCo_{1-x} deposited on a Pt(111) surface. Among ferromagnetic materials, FeCo displays the highest saturation magnetization,[5] while Pt is known to induce large MAE in both Co (Refs. 11 and 12) and Fe.[13] A combination of large M_S and MAE is required to push the superparamagnetic limit to smaller sizes and higher densities while keeping the writing field ($H_{\text{wr}}\approx K/M_S$) in the technological limit. Until now, large MAE values have been predicted and experimentally observed only in distorted FeCo-bct bulk, respectively, several monolayers thick films.[5–7] In a combined experimental and theoretical study we demonstrate that 1-ML-thick Fe_xCo_{1-x} films grown on Pt(111) possess both very large M_S and MAE values compared to most ferromagnetic materials.[14] This result is a consequence of the electronic hybridization between Fe and Co atoms in the monolayer and between the FeCo layer and the Pt(111) substrate.

We find in our calculations in agreement with experiment spin moments of about $3\mu_B$/atom for Fe and $2\mu_B$/atom for Co. These values are only weakly composition dependent, namely, they show a monotonic increase in M_S in going from Co to Fe. This is in contrast with the well-known Slater-Pauling behavior,[15] showing a maximum of M_S at intermediate composition. We attribute this to the reduced film dimensionality which, narrowing the *d*-density of states (DOS), produces a clear splitting of the Fe $3d\uparrow$ and $3d\downarrow$ spin bands. Contrary to the behavior of the spin moments, both the orbital moment and the MAE are found to strongly depend on the alloy composition, with a maximum around the equiatomic stoichiometry. The experiments, in agreement with theory, give a maximum MAE value of 0.5 meV/atom, which is more than 2 orders of magnitude larger than the value measured in bulk bcc FeCo alloy[16] and similar to the values observed in the highly ordered $L1_0$ phase of FePt.[17] Calculations of the element and orbital-resolved DOS clearly demonstrate that the observed composition dependence is the result of Fe-Co electronic hybridization, namely, a fine tuning of the occupation number of spin-down $d_{x^2-y^2}$ and d_{xy} in-plane orbitals, both for Fe and Co, while the population of the $d_{3z^2-r^2}$, d_{xz}, and d_{yz} out-of-plane orbitals remains nearly stable. Moreover, we show that the Pt substrate plays an important role in the Fe-Co hybridization, as well as in determining the MAE and M_S of this system.

II. EXPERIMENT

Fe_xCo_{1-x} films were grown by atomic beam epitaxy from thoroughly outgassed high-purity rods (99.995%) using a commercial electron-beam evaporator. The Pt(111) substrate was prepared by repeated cycles of Ar^+-ion sputtering [1.3 keV at 300 K to remove magnetic layers and at 800 K once the substrate was clean (20 min)], followed by annealing at 800 K at an oxygen partial pressure of $P_{O_2}=6\times10^{-8}$ mbar (10 min) to remove carbon impurities, and final annealing to 1100–1300 K. This preparation procedure gives chemical defect densities below 2×10^{-3} ML and typical terrace sizes of about 1000 Å. Fe and Co atoms were codeposited on the surface. The film coverage and chemical composition were adjusted by varying the Fe and Co fluxes, which were previously calibrated by scanning tunneling microscopy (STM) and x-ray-absorption spectroscopy (XAS) within ±0.05 ML. The evaporation rate for Fe and Co was in the range of 0.1–0.6 ML/min. During deposition the pressure inside the UHV chamber was below 1×10^{-10} mbar. To investigate the effect of the film morphology on the magnetic properties, two types of monolayer films were grown with either a granular or continuous structure.

Granular films have been deposited at $T<50$ K, where surface diffusion of both species is frozen. Their morphologies have been investigated in detail by variable temperature scanning tunneling microscopy (VT-STM) at the Ecole Polytechnique Fédérale de Lausanne (EPFL). Analog growth conditions were used to deposit and investigate *in situ* the granular films by XAS using synchrotron radiation at the ID08 beamline of the European Synchrotron Radiation Facility (ESRF) in Grenoble. XAS experiments were performed in the total electron yield mode using $99\pm1\%$ circularly polarized light and a ±5 T magnetic field generated by a split coil superconducting magnet. The x-ray beam and magnetic field are parallel to each other and form an angle θ with the surface normal. The out-of-plane vs in-plane magnetization was investigated by tilting the sample position from $\theta=0°$ to 70°, corresponding to normal and grazing incidences of the x-ray beam, respectively. All XAS measurements presented here have been performed at 10 K in less than 2 h for each freshly prepared sample. The coverage calibration at the ESRF has been carried out *in situ* by STM after warming up the samples and transferring them from the cryostat to the STM of the ID08 beamline.

Continuous films were investigated by VT-STM and magneto-optical Kerr effect (MOKE) measurements at EPFL. The films were grown at 35 K and then annealed at 300 K for 5 min. MOKE measurements were performed in both polar and transversal configurations as a function of the stoichiometry in the temperature range 35–400 K. An electromagnet with magnetic poles, and a coil inside the vacuum system were used to produce magnetic in-plane and out-of-plane fields at the sample position up to 50 mT. The light source was a *p*-polarized and temperature-stabilized 780 nm laser diode. The angle between the incident beam and the surface normal was 35°. Magnetization curves were acquired by MOKE in temperature intervals of 10 K. A complete characterization of the magnetic properties was always performed in less than 2 h after sample preparation and at a pressure of 4×10^{-11} mbar. A maximum variation in the coercive field of ±1.5 mT was measured when the MOKE experiments were repeated after 2 h. We have taken this value as error bar for the measurements of the coercive field.

III. EXPERIMENTAL RESULTS

A. Structural results: Granular and continuous films

Figure 1(a) shows an STM image of the granular film structure obtained after deposition of 0.6 ML of Co on Pt(111) at 35 K. The observed morphology was independent of the film stoichiometry and of the deposition temperature up to 50 K. Up to this temperature the surface diffusions of Co and Fe are frozen giving rise to statistical growth of islands with density, size, and morphology being independent of composition.[18] From the STM images, we estimated a mean grain diameter of about 20 Å which corresponds to a grain size of about 50 atoms. The grain thickness is one atomic layer; only 0.02 ML is in the second layer. This value implies a low activation energy for interlayer diffusion which is reasonable for the small island sizes of only 8 atoms in diameter. The lattice misfit between Fe and Pt is −10.3% and the one between Co and Pt is −9.4%. Despite these large values STM measurements do not reveal surface partial dislocations in the islands for all stoichiometries, suggesting pseudomorphic growth of the Fe_xCo_{1-x} alloy islands. This can be rationalized by stress relief at the steps,[19] which leads for Co/Pt(111) to an island diameter of 30–40 Å up to which the islands are pseudomorphic and beyond which they have partial dislocations, where the stacking changes from fcc to hcp or vice versa.[20] For Fe on Pt(111) pseudomorphic

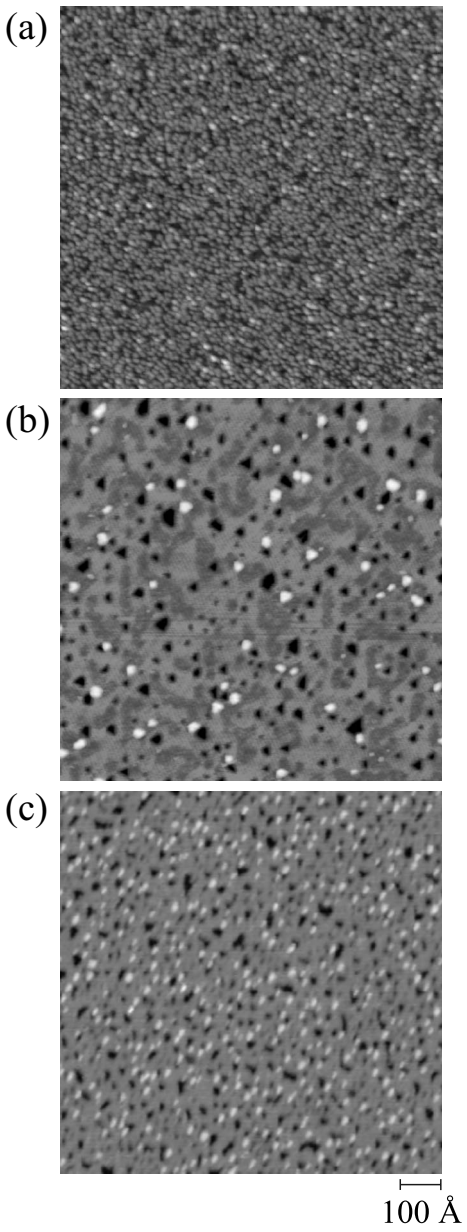

FIG. 1. (a) STM image of 0.60 ± 0.05 ML Co/Pt(111) deposited and imaged at $T=35$ K. The surface exhibits monolayer-thick grains containing on average 50 atoms each. (b) STM image of 1.00 ± 0.05 ML Co/Pt(111). (c) STM image of 1.00 ± 0.05 ML $Fe_{0.40}Co_{0.60}/Pt(111)$. Growth conditions for (b) and (c): deposition at $T=35$ K followed by annealing for 5 min at $T=300$ K.

growth has been observed up to completion of the first monolayer.[21] This is surprising in view of the large misfit and implies large tensile stress.

Continuous films were grown by depositing 1 ML of Fe_xCo_{1-x} at temperatures lower than 50 K followed by annealing at 300 K. This procedure presents two advantages in comparison with deposition directly at room temperature. First, the film morphology is composition independent as diffusion is entirely frozen for both elements during deposition, and second the morphology is coming closest to an ideal flat and defect-free single layer. Examples are shown in Fig. 1 for monolayers formed of pure Co and of $Fe_{0.40}Co_{0.60}$.

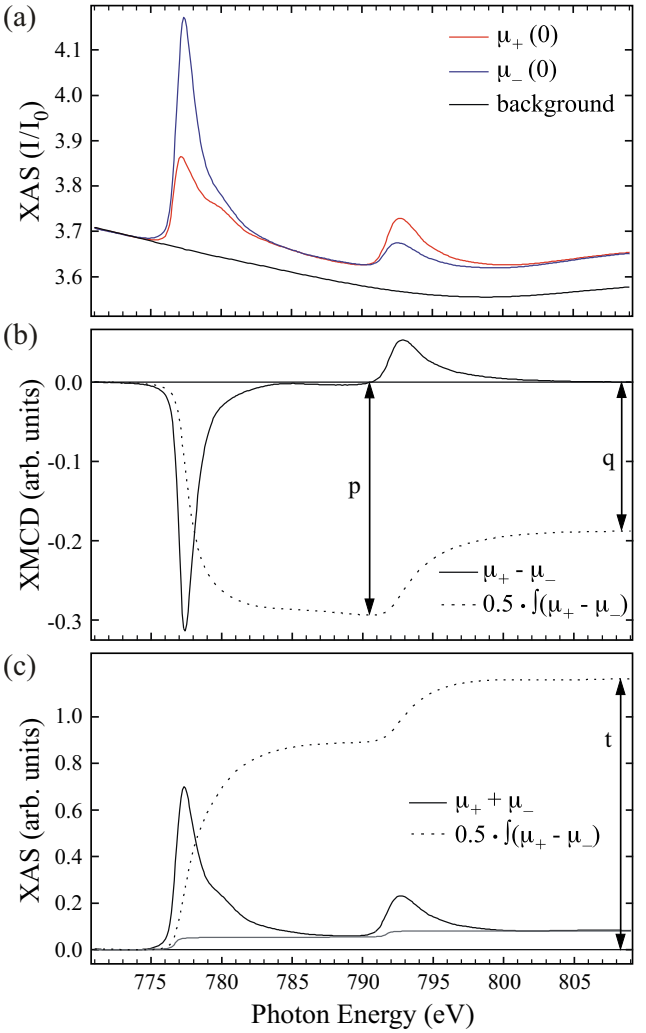

FIG. 2. (Color online) XAS and XMCD spectra recorded at the Co $L_{2,3}$ edges for a 0.83 ± 0.05 ML film of $Fe_{0.35}Co_{0.65}$ ($T=10$ K, $\mu_0 H=5$ T, field and beam normal to the sample corresponding to $\theta=0°$). (a) Absorption spectra normalized to the incident photon flux (I_0) for parallel ($\mu_+=I_+/I_0$) and antiparallel ($\mu_-=I_-/I_0$) alignment of photon helicity with respect to the field. The shown background signal corresponds to the XAS acquired on the clean Pt(111) surface. (b) XMCD spectrum with the corresponding integral calculated from spectra shown in (a). (c) Total XAS spectra with the corresponding integral calculated from spectra shown in (a) after subtraction of the background signal and of the two-step function accounting for nonresonant absorption (full gray line).

Second layer coverage represents less than 4% of the total coverage [for comparison second layer coverage amounts to about 30% in room temperature deposited 1 ML of Co (Ref. 22) and 1 ML of Fe (Ref. 21)]. The density of second layer islands and first layer vacancies was only 8×10^{-3} ML, and this is independent of stoichiometry. This allows minimization of the effect of film roughness on the magnetic properties.[23,24] Randomly distributed partial surface dislocations are observed for all compositions, except for pure Fe. The dislocations are the domain walls separating fcc from hcp staking areas and appear in pairs due to the energy difference between the two stacking sequences. Depending on the tip conditions, these pairs appear as a bright double line

TABLE I. Element-resolved orbital and spin moments (in units of μ_B/atom) estimated from XAS data acquired along the easy axis (θ=0°) with $\mu_0 H$=5 T. m_L and $m_{S_{\text{eff}}}$ are the average orbital and effective spin moments per atom in the alloy. The saturation magnetization M_S and the total magnetization at 5 T, $M_{5\ \text{T}}$, are estimated from the magnetization curves in Fig. 3. The values for pure Co correspond to 1-ML-high Co islands with an average size of 40 atoms and are taken from Ref. 8.

	Θ (ML)	L_{Fe}	$(S_{\text{eff}})_{\text{Fe}}$	$(L/S_{\text{eff}})_{\text{Fe}}$	L_{Co}	$(S_{\text{eff}})_{\text{Co}}$	$(L/S_{\text{eff}})_{\text{Co}}$	m_L	$m_{S_{\text{eff}}}$	$M_{5\ \text{T}}/M_S$
Co	Ref. 8				0.31 ± 0.06	1.8 ± 0.1	0.17 ± 0.02	0.31 ± 0.06	1.8 ± 0.1	1
$Fe_{0.35}Co_{0.65}$	0.83 ± 0.05	0.30 ± 0.03	3.0 ± 0.3	0.10 ± 0.02	0.50 ± 0.05	2.2 ± 0.2	0.23 ± 0.04	0.43 ± 0.08	2.5 ± 0.5	1
$Fe_{0.52}Co_{0.48}$	0.73 ± 0.05	0.24 ± 0.02	2.1 ± 0.2	0.11 ± 0.02	0.40 ± 0.04	1.7 ± 0.2	0.24 ± 0.03	0.32 ± 0.06	1.9 ± 0.4	0.85
$Fe_{0.55}Co_{0.45}$	1.17 ± 0.05	0.29 ± 0.03	2.9 ± 0.3	0.10 ± 0.02	0.48 ± 0.04	2.2 ± 0.2	0.22 ± 0.03	0.38 ± 0.07	2.6 ± 0.5	1
Fe	0.79 ± 0.05	0.14 ± 0.02	1.2 ± 0.2	0.12 ± 0.04				0.14 ± 0.02	1.2 ± 0.2	0.85

or as a depression, as in Fig. 1. In both cases the positive or negative apparent height amounts to 0.25 ± 0.05 Å. Although surface dislocations have been observed for pure Co (Ref. 22) but not for pure Fe,[21] a clear correlation between dislocation density and film chemical composition could not be detected. This finding is in agreement with the random chemical order due to the growth by codeposition at temperatures low enough to suppress surface diffusion.

Experiments carried out above room temperature revealed structural evolutions such as segregation of adatoms on top of the first layer. Previous experimental and theoretical studies were focused on the structural evolutions occurring above room temperature, e.g., insertion of atoms in the substrate,[22] intermixing,[25–27] or adatom segregation at the film surface.[28] In order to have monolayers of well-defined composition and structure we restrict ourselves to the temperature range where structural evolution is absent.

B. X-ray-absorption spectroscopy on granular Fe_xCo_{1-x} films: Magnetic moments versus stoichiometry

We investigated four different compositions, all of them showing intense dichroic signals. XAS spectra were acquired at the $L_{3,2}$ edges of both Fe and Co. As an example, Fig. 2 shows the XAS spectra recorded at the Co $L_{3,2}$ edges for a 0.83-ML-thick granular film of $Fe_{0.35}Co_{0.65}$ for both helicities in a magnetic field of $\mu_0 H$=5 T. Figure 2(a) represents the raw absorption spectra normalized to the incident photon flux for parallel (μ_+) and antiparallel (μ_-) alignment of photon helicity with respect to the applied magnetic field. Spectra recorded on the Pt(111) substrate are shown as background in Fig. 2(a). Figures 2(b) and 2(c) show the resulting x-ray magnetic circular dichroism (XMCD) ($\mu_+-\mu_-$) and XAS ($\mu_++\mu_-$) intensities together with their integrals. In addition to the substrate contribution, a two-step function, taking into account nonresonant absorption shown in Fig. 2(c), has to be subtracted from the XAS signal in order to isolate the contribution of the $2p\rightarrow 3d$ transitions. According to the XMCD sum rules, the projections of the orbital L (Ref. 29) and effective spin $S_{\text{eff}}=S+7D$ magnetic moments[30] onto the incident light direction can be determined from the XMCD and XAS spectra as follows:

$$L=-\frac{4}{3}h_d\frac{\int_{L_3+L_2}(\mu_+-\mu_-)dE}{\int_{L_3+L_2}(\mu_++\mu_-)dE}=-\frac{4}{3}h_d\frac{q}{t}, \tag{1}$$

$$S+7D=-h_d\frac{6\int_{L_3}(\mu_+-\mu_-)dE-4\int_{L_3+L_2}(\mu_+-\mu_-)dE}{\int_{L_3+L_2}(\mu_++\mu_-)dE}=-h_d\frac{6p-4q}{t}, \tag{2}$$

where h_d is the number of holes in the $3d$ states, D is the spin magnetic dipole moment, and the integrals p, q, and t are labeled in Fig. 2. The resulting out-of-plane magnetic moments for Fe and Co are shown in Table I for the different stoichiometries. For the evaluation of L and S_{eff}, we assumed h_d=2.4 for Co (Ref. 8) and h_d=3.4 for Fe.[31] This assumption simplifies the comparison of the magnetic moments with previous literature values. The uncertainty on the number of unoccupied $3d$ states can generally be quite large. Variations on the order of 10% can arise from the h_d dependence on the alloy stoichiometry[32] and from the reduced dimensionality.[33] However, our calculations give with h_d=2.3 for Co and h_d=3.4 for Fe (see Sec. IV) values in excellent agreement with the two previous values from literature. In addition, these values vary by less than 2% with the alloy composition. Therefore we estimate in the present case the uncertainty on h_d to be small, and the error bars for L and S_{eff} have been derived taking into account only the experimental errors.

The orbital moments of Co and Fe show a strong dependence on the alloy stoichiometry. This dependence is even larger when considering the mean orbital moment per alloy atom, defined as $m_L=xL_{\text{Fe}}+(1-x)L_{\text{Co}}$, with a minimum of $(0.14\pm0.02)\mu_B$/atom for pure Fe and a maximum of $(0.43\pm0.08)\mu_B$/atom for x=0.35 and $(0.31\pm0.06)\mu_B$/atom for pure Co (see Table I). In contrast, the mean effective spin moment $m_{S_{\text{eff}}}$ shows only a slight dependence on the film stoichiometry and tends to increase moving from Co to Fe.

The only exception is the pure Fe film for which we measure a strongly reduced effective spin moment of $S_{\text{eff}} = (1.2 \pm 0.2)\mu_B/\text{atom}$ (see Sec. V B).

C. Granular films: Magnetization curves and magnetic anisotropy energy

The magnetization curves in Fig. 3 represent the peak of the Fe (Co) L_3 XMCD intensity at 707.2 (777.3) eV divided by the pre-edge XAS intensity at 704.0 (773.0) eV as a function of the external magnetic field for $\theta = 0°$ and 70°. Normalization to the pre-edge intensity compensates for the angular and field dependence of the total electron yield of the sample, which strongly affect the absolute photocurrent.

The shape of the $M(H)$ curves measured with $\theta = 0°$ and 70° shows that all the samples exhibit an out-of-plane easy axis. Figures 3(a) and 3(b) show magnetization curves of pure Fe and $Fe_{0.52}Co_{0.48}$, both are not saturated at the maximum available magnetic field of 5 T. In order to estimate the saturated magnetic moment per atom, we linearly extrapolated $M(H)$ above 4 T and defined the intersection point of the magnetization curves measured along the two directions as M_S. For the nonsaturated samples we found that the magnetization at $\mu_0 H = 5$ T is about 85% of M_S. Note that the effective spin and orbital moments reported in Table I are the ones measured at $\mu_0 H = 5$ T. In alloy samples we find that the Fe and Co magnetization curves coincide, as expected because of the strong ferromagnetic exchange coupling between the two species [see Fig. 3(b)].

It is interesting to compare Figs. 3(b) and 3(c), which refer to samples with very similar chemical compositions but different coverages. The film with $\Theta = 0.73 \pm 0.05$ ML shows reversible magnetization curves, while the one with $\Theta = 1.17 \pm 0.05$ ML shows hysteresis with a coercive field H_c of about 1 T. The origin of this difference resides in the film morphology. As pointed out above, the growth conditions of the granular films are to a good approximation ideal statistical growth with frozen surface diffusion. In this case, island percolation occurs at a coverage of $\Theta \approx 0.9$ ML.[34] In other words, for coverages below this value the film can be seen as an ensemble of monolayer-high magnetically independent particles, while for coverages above the film becomes a continuously connected structure. Because in ultrathin films with out-of-plane easy axis the critical single-domain diameter is on the order of 1 μm (Refs. 35 and 36), one expects that the morphological percolation is accompanied by the onset of irreversible mechanisms of magnetization switching, such as nucleation of reversed domains and domain-wall propagation.

The films with coverage below the coalescence threshold have the advantage that the mechanism of magnetization reversal is the rotation of the magnetization vector of each island, and therefore one can straightforwardly derive the MAE from the angular dependence of the magnetization curves $M_\theta(H)$ using the following equation:[37,38]

$$\text{MAE} = \frac{\int_0^{M_S} \mu_0 H dM_{\theta_1} - \int_0^{M_S} \mu_0 H dM_{\theta_2}}{\sin^2(\theta_1 - \theta_2)}, \qquad (3)$$

where H is the applied magnetic field, $\theta_1 = 0°$ and $\theta_2 = 70°$. M_S is shown in Table I as a multiple of $M_{5\text{ T}}$, the total

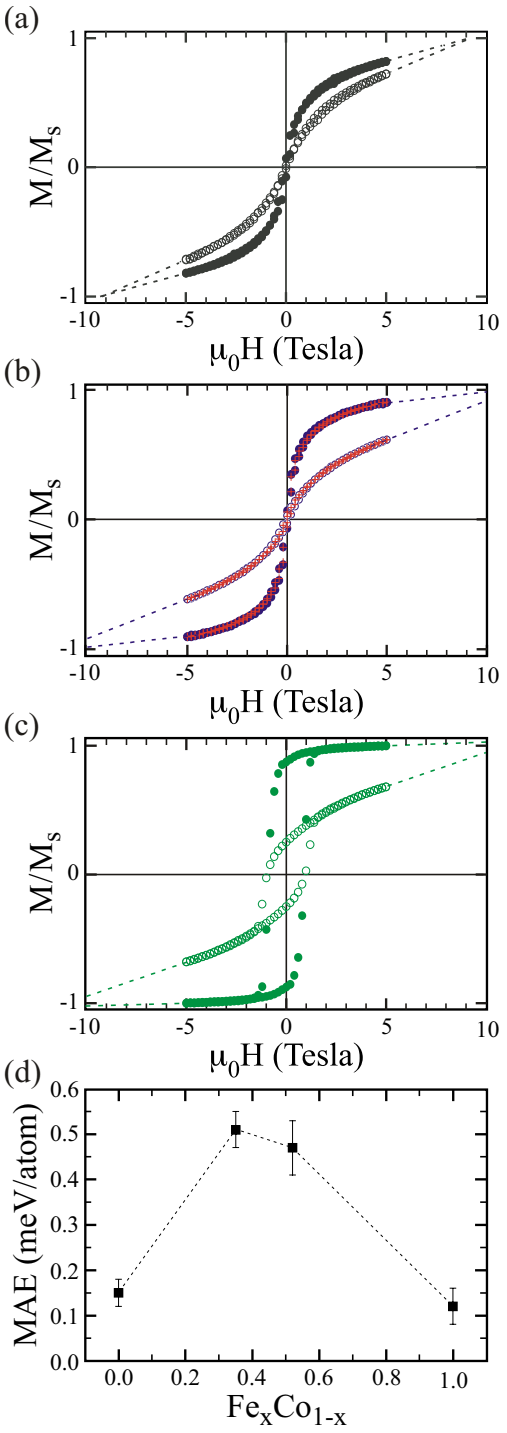

FIG. 3. (Color online) Magnetization curves $M_\theta(H)$ of granular films measured at the Fe edge at $T = 10$ K, $\theta = 0°$ (solid circles), and $\theta = 70°$ (open circles) normalized to M_S (see text). (a) $\Theta = 0.79 \pm 0.05$ ML pure Fe; (b) $\Theta = 0.73 \pm 0.05$ ML $Fe_{0.52}Co_{0.48}$, crosses represent the Co edge data; (c) $\Theta = 1.17 \pm 0.05$ ML $Fe_{0.55}Co_{0.45}$. Dotted lines are linear extrapolations of the experimental data when saturation is not reached. (d) MAE vs stoichiometry calculated from Eqs. (3) and (4). The value for pure Co is taken from Ref. 8 and corresponds to one-monolayer-thick Co islands with an average size of 40 atoms. The dotted line is a guide for the eyes.

magnetic moment estimated at 5 T following

$$M_{5\ T} = x[L_{\mathrm{Fe}} + (S_{\mathrm{eff}})_{\mathrm{Fe}}] + (1-x)[L_{\mathrm{Co}} + (S_{\mathrm{eff}})_{\mathrm{Co}}] + m_{\mathrm{Pt}}. \tag{4}$$

Equation (4) takes into account the orbital and spin moments of Fe and Co, weighted by the film stoichiometry, and the magnetic moment induced in the substrate Pt atoms. Our calculations (see Sec. IV B) give $m_{\mathrm{Pt}}=(0.25\pm0.03)\mu_B$/atom, slightly decreasing when moving from pure Co to pure Fe. These values are consistent with previous studies which found $m_{\mathrm{Pt}}\simeq 0.2\mu_B$/atom (Ref. 25) and $m_{\mathrm{Pt}}\simeq 0.27\mu_B$/atom (Ref. 39) for the induced Pt moment in Co/Pt(111) and Fe/Pt(111), respectively.

A strong dependence of the MAE on the alloy composition is observed in Fig. 3(d). We find a maximum of 0.50 ± 0.05 meV/atom for close to equiatomic stoichiometry. This value is about three times the values measured for pure Fe (0.1 ± 0.05 meV/atom) and Co (0.15 ± 0.02 meV/atom) monolayers on Pt(111).

D. Continuous Fe_xCo_{1-x} films: Coercivity versus stoichiometry

The magnetization of continuous films deposited at 35 K and annealed to room temperature was studied by means of *in situ* MOKE. In large islands or continuous films, magnetization reversal does not take place by coherent rotation but by the energetically favored nucleation and growth of reversed domains. Consequently, the measured coercive fields $H_c(T)$ may be orders of magnitude smaller than the values estimated from the MAE assuming coherent magnetization rotation. However, because the continuous films investigated here all have similar morphology (see Sec. III A), H_c may be used to monitor relative changes in the MAE as a function of film stoichiometry.

All the measured samples showed square-shaped hysteresis loops for the out-of-plane magnetization measured by polar Kerr effect [Fig. 4(a)]. Using transverse Kerr effect no in-plane signal was observed within the detection limit. From these observations we deduce an out-of-plane easy axis of magnetization and a single-domain remanent state, independent of film stoichiometry.

The coercive field measured at $T=240$ K is shown in Fig. 4(b) as a function of stoichiometry of the monolayers. For pure Co ($x=0$), the coercive field amounts to $\mu_0 H_C = 24.5\pm1.5$ mT and for pure Fe ($x=1$) to 4.5 ± 1.5 mT. Mixing the two elements produces an increase in the switching field up to a maximum of $\mu_0 H_C=43.5\pm1.5$ mT. The $H_c(x)$ trend is very similar to the one observed for the MAE of granular films with the maximum reached in both cases at $x=0.40$.

Magnetization curves at different temperatures for a pure Fe film are shown in Fig. 5(a). The coercive field vanishes at 260 K and the loops become *s* shaped at 270 K, suggesting the occurrence of a magnetic phase transition associated with the Curie temperature T_C. At T_C the susceptibility $\chi=M/H$ diverges. Therefore T_C can be determined by linearly extrapolating the magnetization curve data represented in an Arrot plot $M^2(H/M)$ to zero.[40–42] From Fig. 5(b) we deduce $T_C=270\pm5$ K for the pure Fe film. For all the other stoichiometries, T_C is above 300 K but below 400 K as inferred from extrapolating from the temperature dependence of $H_c(T)$. We already discussed the impossibility to experimentally verify these results because the samples undergo structural changes when annealed to temperatures higher than 320–340 K (see Sec. III A). As expected due to the low dimensionality of the studied films, the measured values of T_C are strongly reduced with respect to the bulk values of 1043 K for Fe and 1388 K for Co.[43] Alloying Fe and Co has been shown to increase T_C.[44,45] Finally, we note that the observed behavior differs from what has been reported for Fe_xCo_{1-x} monolayers on W(110). In that case the authors observed a monotonically decreasing Curie temperature with increasing the Co concentration.[46] This was ascribed to the Fe-Co hybridization which, in this peculiar system, reduces the tendency toward ferromagnetic ordering with increasing Co content.[47]

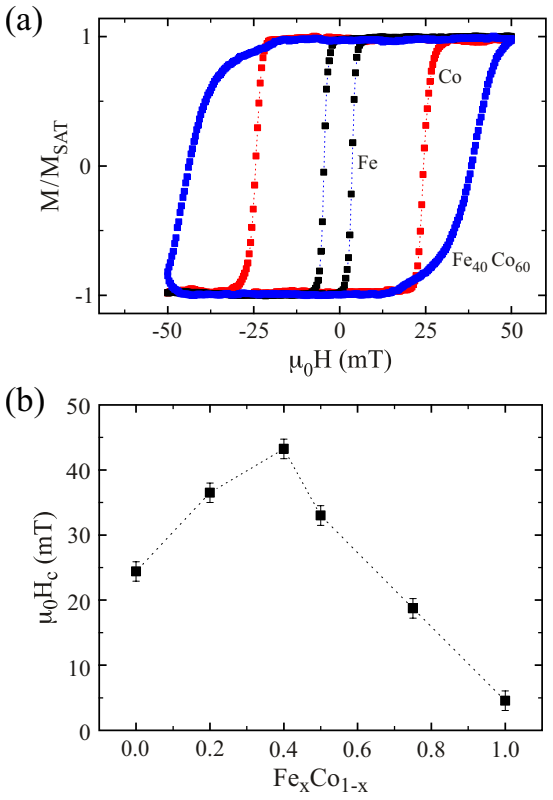

FIG. 4. (Color online) (a) Polar MOKE magnetization curve recorded at $T=240$ K for 1.00 ± 0.05 ML Co (red), Fe (black), and $Fe_{0.40}Co_{0.60}$ alloy (blue). (b) Coercive field vs stoichiometry for 1 ML of Fe_xCo_{1-x} measured along the easy axis ($T=240$ K). The dotted line is a guide for the eyes.

IV. THEORY

A. Computational method

In order to gain further insight into the magnetic properties of this system we performed first-principles electronic structure calculations using the screened Korringa-Kohn-Rostoker (SKKR) Green's-function method.[48] In this approach a surface is described as a system with two-

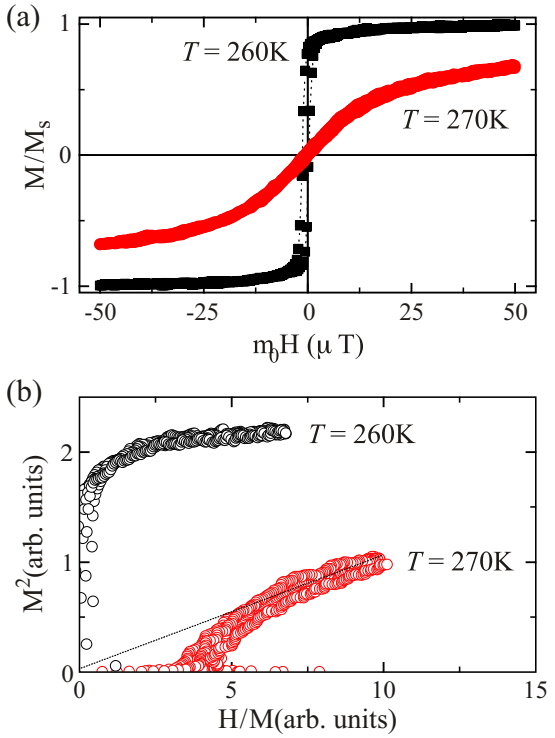

FIG. 5. (Color online) (a) Polar MOKE magnetization curves recorded at T=260 and 270 K for 1.00±0.05 ML Fe deposited on Pt(111) at 35 K and annealed to 300 K. (b) Arrot-Kouvel plot for the same sample at T=260 and 270 K. The Curie temperature T_C is determined when the linearly extrapolated high-field data intercept the origin (solid line).

dimensional translational symmetry. In the third direction it consists of a semi-infinite bulk on one side and of a semi-infinite vacuum region on the other. The relativistic scattering solutions, and consequently the Green's functions, are obtained by solving the Dirac equation, whereby spin-orbit coupling is automatically included in the calculations. Wave functions and scattering matrices have been calculated up to an orbital momentum quantum number of $\ell_{\max}=2$. This choice of $\ell_{\max}=2$ means that s, p, and d valence electrons have been taken into account. The potentials are described in the atomic sphere approximation (ASA) and within the local spin-density approximation (LSDA). When calculating the electrostatic potential by solving Poisson's equation, moments of the charge density up to $\ell_{\max}=4$ have been considered in order to realistically describe the potentials and energies in the layers at and near the surface. For the self-consistent calculations, 80 $k_{\|}$ points have been used in the irreducible surface Brillouin-zone (ISBZ) integrations and 16 energy points for the energy integrations along a semicircular contour in the complex energy plane by means of a Gaussian quadrature. The magnetocrystalline anisotropy energies have been obtained by means of the force theorem as the corresponding difference in band energies[49] which have been converged in terms of k points in the ISBZ (for details see Ref. 50).

The geometry of the studied system was chosen such that 1 ML of Fe_xCo_{1-x} has in a first approach been placed onto positions following the stacking sequence of the Pt(111) surface; cf. Fig. 6. As lattice constant the experimental value for Pt (a_0=3.92 Å) was used. Since a considerable mismatch between the lattice constants of Pt and Co and Pt and Fe of about 10% exists, the influence of the relaxation of the interlayer spacing between overlayer and substrate on the magnetocrystalline anisotropy energy has been investigated.

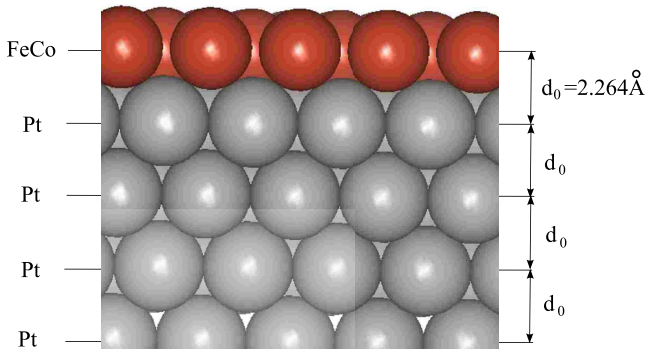

FIG. 6. (Color online) Geometry of the system studied by means of SKKR calculations. 1 ML of FeCo with varying composition has been placed on top of an ideal Pt(111) surface.

All calculated quantities have been studied as a function of the composition of the Fe_xCo_{1-x} monolayer by employing the coherent-potential approximation (CPA), which treats the Fe-Co system as a disordered alloy. The effects of interdiffusion and roughness have not been considered in the theoretical investigations.

B. Spin and orbital magnetic moments

The spin and orbital magnetic moments have been calculated as a function of Fe concentration x. Figure 7 illustrates that the average spin magnetic moment, $m_S=xS_{\mathrm{Fe}}+(1-x)S_{\mathrm{Co}}$ is a linear function of the Fe concentration, which is a characteristic that has previously been documented for monolayers of Fe_xCo_{1-x} on a Cu(100) substrate.[51] The individual Fe and Co spin moments are only a very weak function of the alloy composition. This is in contrast to a bulk Fe-Co alloy where the average magnetic moment, accordingly to the Slater-Pauling model,[15] exhibits a maximum at about 30% of Co content because of the strong concentration dependence of the local Fe moments. In comparison with the bulk, the magnetic moments of both Fe and Co are considerably enhanced in the monolayer on Pt(111). The spin moment of Fe is about 3.0μ_B (2.2μ_B in bulk) and that of Co is about 2.0μ_B (1.6μ_B in bulk).

Turning our attention to the orbital magnetic moments one finds, in contrast to the spin moments, a strong dependence on the alloy composition. Furthermore, a considerable enhancement of the orbital moments in comparison to the respective bulk values is predicted. The LSDA bulk values for the orbital moments of Fe and Co are 0.043μ_B and 0.078μ_B, respectively. The values shown in Fig. 7 correspond to an increase in the moments by a factor of approximately 2 for the Co atoms and by a factor of 3 for the Fe atoms compared to these bulk values.

The deposition of magnetic atoms induces magnetic moments in the Pt substrate, known to be highly polarizable.

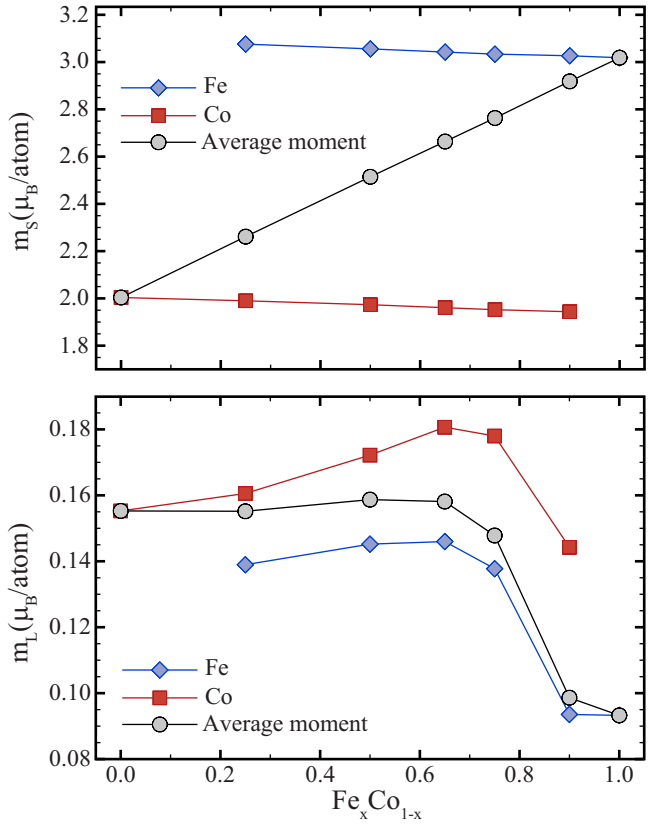

FIG. 7. (Color online) Spin and orbital magnetic moments as functions of Fe concentration x. Individual and averaged values are plotted. m_L values are the ones calculated along the easy axis (see Sec. IV C). Note the linear dependence of the average spin moments on x in contrast to what is observed in the bulk bcc FeCo alloy. The lines are guides for the eyes.

The total induced moment per Pt atom of the topmost layer ranges from about $0.23\mu_B$ for a pure Fe layer to $0.28\mu_B$ for a pure Co layer (Fig. 8). Both orbital and spin Pt moments are collinear with the magnetization of alloy film.

C. Magnetocrystalline anisotropy energy

The magnetocrystalline anisotropy energy has been calculated as the difference in band energy, $E_b(\theta,\phi)$, for two magnetization directions, θ=0° and 90°, corresponding to easy and hard magnetization axis. For θ=90° there exists a dependence of the band energy difference on the azimuthal angle ϕ, which is, however, several orders of magnitude smaller (on the order of a few μeV). In order to determine the MAE, we have therefore calculated

$$\mathrm{MAE} = \Delta E_b^{x-z} = E_b(90\,^\circ, 0^\circ) - E_b(0\,^\circ, 0^\circ). \qquad (5)$$

The resulting MAE is plotted in Fig. 9 as a function of Fe concentration. Note that the dipolar energy is not taken into account. The maximum energy appears at $Fe_{0.5}Co_{0.5}$ and the easy axis is parallel to the surface normal, as long as the concentration of Fe atoms is below approximately 75%. Beyond this concentration the calculations predict in-plane magnetization with a total MAE of −0.71 meV for the pure Fe film.

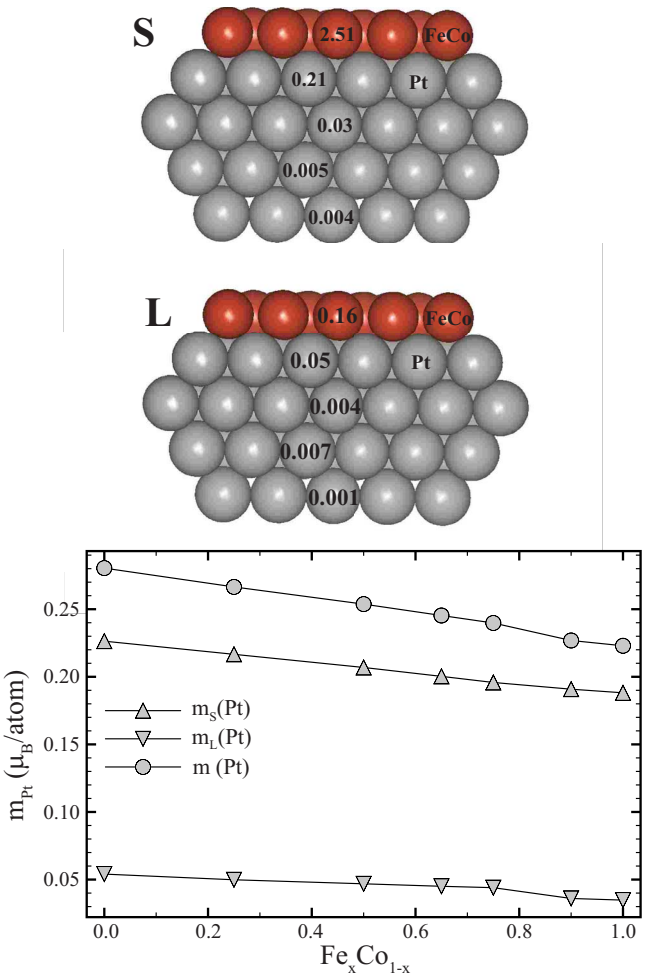

FIG. 8. (Color online) (Bottom) Induced spin and orbital moments in Pt atoms of the topmost substrate layer as a function of Fe concentration x. Lines are guides for the eyes. The layer-resolved induced spin (top) and orbital (middle) moments (in units of μ_B) in Pt atoms up to the fourth substrate layer for the $Fe_{0.5}Co_{0.5}$ monolayer are shown.

D. Contribution of the Pt substrate

It is of interest to assess the contribution of the substrate to the total MAE. According to the calculations, this contribution is always favoring in-plane magnetization and it has an almost linear function of the Fe concentration (see Fig. 9). The energy attributed to the Pt substrate is by a factor of 10 larger for a pure Fe than for a pure Co monolayer. Except for a pure Fe film the Fe_xCo_{1-x} film contributes with positive-energy values, hence favoring perpendicular magnetization.

E. Effect of layer relaxation

Because of the about 10% lattice mismatch between Fe and Co bulk nearest neighbor distance and the one of Pt one might expect a contraction of the distance between the last layer of the Pt substrate and the magnetic overlayer. Technically this has been realized in the simulation by changing only the distance between the last Pt and the overlayer, cf. Fig. 6. Consequently the volume of the Wigner-Seitz cell—and hence that of the ASA sphere—of the Pt atoms in the

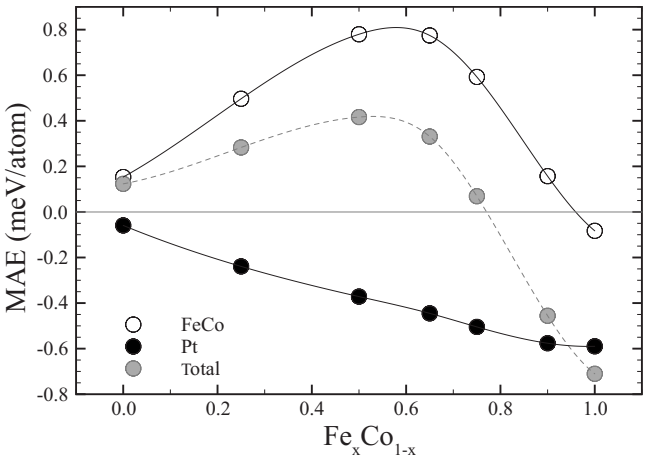

FIG. 9. MAE as function of Fe concentration x. The separated contribution of the Pt substrate, per Pt surface atom, (filled circles) and of the Fe_xCo_{1-x} overlayer (empty circles) to the total MAE (gray circles: dashed line) are also shown. Lines are guides for the eyes.

topmost layer were reduced, and those of the Fe and/or Co atoms remained unchanged. The influence of a successive change in this interlayer distance on the MAE is illustrated in Fig. 10. The results suggest that the MAE is strongly affected by changes in the interlayer distance. In particular, in the regime between $40\% < x < 80\%$, the MAE can even change its sign depending on the relaxation value. Generally, the MAE is more positive when the film is outward relaxed which is expected since the Pt substrate induces in-plane MAE.

V. DISCUSSION

A. Experiment versus theory

Rather good agreement is found for all compositions apart from clean Fe between experimental data and theoretical calculations for the magnetic moments. This is surprising since theory treats a perfect monolayer, whereas the XMCD measurements have been performed on granular films. The spin moment (per alloy atom) is predicted by theory to linearly increase from $m_S=2.0\mu_B$ to $m_S=3.0\mu_B$ while moving from pure Co to pure Fe. XMCD data give an effective spin moment of $S_{\text{eff}}=(1.8\pm0.1)\mu_B$ for pure Co which increases by increasing Fe content. For $Fe_{0.55}Co_{0.45}$ we measure $m_{S_{\text{eff}}}=(2.6\pm0.5)\mu_B$, in coincidence with theory and similar to the bcc bulk value $(2.3\mu_B)$. Slightly smaller values were recently reported for $Fe_{0.55}Co_{0.45}$/Pt superlattices $(2.5\mu_B)$,[52] three-dimensional (3D) crystalline $Fe_{0.56}Co_{0.44}$ nanoparticles $(2.3\mu_B)$,[53] and a significantly smaller one for 6-ML-thick FeCo films on Rh(100) close to the equiatomic composition $(1.8\mu_B)$.[7]

An evident discrepancy between theory and XMCD data exists in the case of pure Fe for which we measured a strongly reduced effective spin moment of $S_{\text{eff}}=(1.2\pm0.2)\mu_B$ vs $3.0\mu_B$ found by theory. The experimental value is also substantially lower than $2.5\mu_B$ reported in FePt nanoparticles[54,55] and multilayers.[56] Low spin values have been reported for 1 ML of Fe on Cu(111) (Refs. 57 and 58) and on Au(111).[59] This is probably the consequence of complex magnetic structures with prevalent antiferromagnetic (AFM) order characterizing thin Fe film with strained fcc structures, as recently observed for the Fe ML on Ir(111).[60] Because the lattice constant of Ir and Pt differs by only 2% and because they are both highly polarizable, it is possible that similar AFM structures also form on the Pt(111) surface. Our calculations assumed ideal flat films pseudomorphic with the Pt(111) surface and cannot account for such low moment structures. When adding Co atoms, the strong ferromagnetic behavior of Co on Pt(111) and the strong hybridization between Fe and Co restore the ferromagnetic order at the Fe sites.

The orbital moment is seen in experiment and theory to have a maximum close to $x=0.5$. The exact composition where this maximum is taken on varies slightly between theory, $x=0.6$, and experiment, $x=0.4$. Moreover, theory substantially underestimates m_L with respect to experiment. This is not surprising because the local-density approximation used for the present calculations typically underestimates the orbital magnetic moments of $3d$ metals by about a factor of 2. Arguably, correlation effects may play a prominent role in correctly predicting the magnitude of the orbital polarization.[61] However, the general trend observed as a function of the film stoichiometry should not be affected. Comparing again with the 6-ML-thick FeCo films on Rh(100) we note that also in that case a similar behavior for m_L was observed with a maximum at $x=0.4$.[7]

The MAE also shows minima for pure Fe and pure Co composition and has a maximum value of about 0.5 meV/atom for a film stoichiometry close to the equiatomic composition. It is worth nothing that this value is orders-of-magnitude enhanced compared with the bcc Fe and hcp Co bulk values of 5 and 45 μeV/atom, respectively.[14,62] The observed bell-shaped behavior as a function of the film stoichiometry is very similar to what has recently been predicted and measured in films of a few nanometer thickness.[5–7] Our experimental and theoretical results dem-

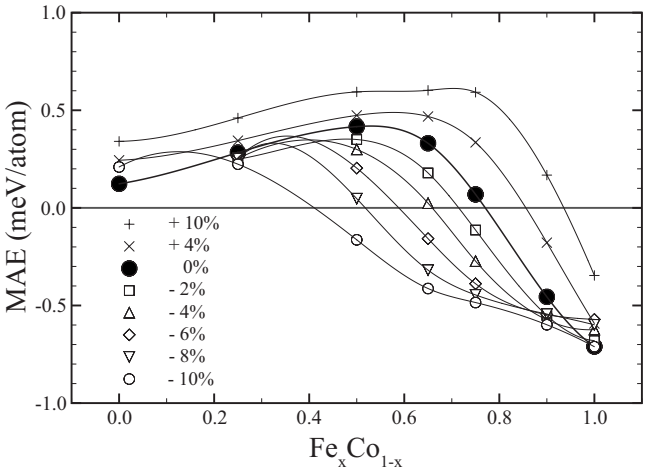

FIG. 10. Total MAE as function of the interlayer distance between the magnetic film and the topmost Pt layer. The interlayer distance is expressed in percentage of the substrate interlayer distance. Lines are guides for the eyes.

onstrate an out-of-plane MAE for the FeCo films. However, a clear discrepancy exists for the pure Fe film MAE which is found out of plane in the experiments and predicted in plane by the calculations. This is predominantly due to the strong in-plane contribution of the Pt substrate found in the calculations (see Fig. 9). Figure 10 also shows that the interlayer relaxation of the Fe film with respect to the Pt(111) substrate is not responsible for the predicted in-plane easy axis. The calculations find for the Fe monolayer much higher spin moments than the experimentally observed ones, which certainly affects the spin-orbit interaction between film and substrate and consequently the MAE of the system.

B. Electronic structure analysis

The bcc FeCo alloy is one of the most studied B2 alloys. Its magnetization as a function of the Co concentration is well described by the Slater-Pauling curve which shows a maximum at about 30% of Co and then a decrease by further increasing the Co content.[15] This can be understood, taking into account that Fe is a weak ferromagnet with the Fermi level intersecting both the $3d\uparrow$ and $3d\downarrow$ spin bands, while Co is a strong ferromagnet having holes only in the $3d\downarrow$ band. The strong hybridization of Fe and Co in the alloy produces two concomitant effects. The first is an increase in the Fe exchange splitting relative to pure Fe. The second is that the large Co electron-electron interaction to bandwidth ratio assists and strengthens the weaker Fe electron-electron interaction by saturating the Fe moment. The net result is a redistribution of $3d\downarrow$ electrons to the $3d\uparrow$ states at the Fe sites while adding Co up to a concentration of about 30%. After reaching the maximum magnetization value, the total number of $3d\uparrow$ electrons remains constant, whereas the number of $3d\downarrow$ electrons increases in order to accommodate the additional electrons coming from Co.[32,63–65]

Our experimental and theoretical data support a different behavior for the Fe_xCo_{1-x} monolayer film on Pt(111). Calculations predict a linear decrease in the average spin moment m_S moving from pure Fe to pure Co, as illustrated in Fig. 7. The spin-resolved DOS of Fe (Co) demonstrates that the spin-up band is almost completely filled, with about 4.8 electrons, while about 1.8 (2.9) electrons are localized in the spin-down band, independently on the Co concentration. Consequently, the spin moment at both the Co and Fe sites is composition independent, and the alloy magnetization is simply given by the weighted mean of Fe and Co spin moments. This is also partially seen in the experimental data giving a spin moment $S_{\text{eff}}=(1.8\pm0.1)\mu_B$ for Co which increases to $m_{S_{\text{eff}}}=(2.6\pm0.5)\mu_B$ for $Fe_{0.55}Co_{0.45}$. The reason for this different behavior with respect to the bulk can be easily understood by comparing the d band of the Fe monolayer (see Fig. 11) with that of bulk Fe [see Fig. 2(b) of Ref. 65]. Two features in the bulk DOS are evident: a small peak at the Fermi energy E_F in the majority states (absent in the film) and a clear peak below E_F in the minority states (crossing E_F in the film). This strong superposition of minority and majority states is responsible for the reduced spin moment observed in bulk Fe. In the monolayer film, the d-band narrowing due to the reduced symmetry produces a clear splitting of majority and minority states, forcing the Fe to behave as a strong ferromagnet. Adding Co atoms strengthens the d-band narrowing, as seen in Fig. 11 by comparing the DOS of pure Fe and $Fe_{0.5}Co_{0.5}$ films. However, because the Fe spin moment is already close to the maximum value given by a completely filled $3d\uparrow$ shell, adding Co atoms plays only a fractional role.

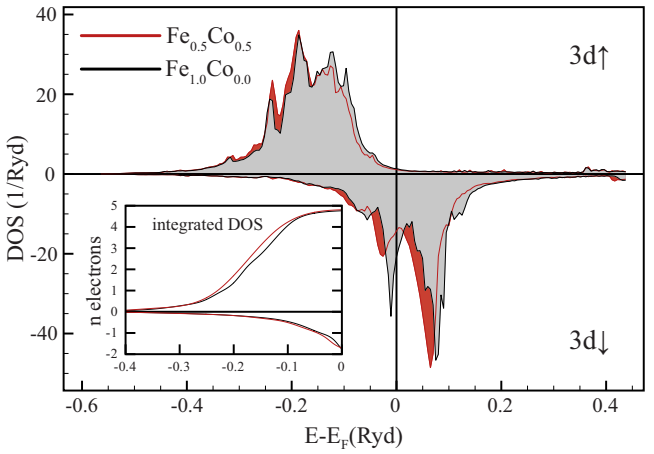

FIG. 11. (Color online) Calculated Fe DOS for $Fe_{0.50}Co_{0.50}$ and for pure Fe monolayer films. The inset shows the corresponding integrated DOS (1 Ryd=13.6 eV).

Let us now consider what happens for the orbital moment L and the MAE, related to L via the spin-orbit interaction. In bulk, the high symmetry of the bcc structure strongly quenches L with the consequence that also the MAE is close to zero. Large MAE values can only be observed in highly strained bct structures which destroy the translational symmetry of the bcc structure. The unquenched orbital moment due to the reduced symmetry is accompanied by an anisotropy of the orbital moment itself which in turn generates a large value of the MAE via the spin-orbit coupling. In particular for bulk FeCo alloys it has been shown that a tetragonal distortion of the bcc structure produces a reduction in the energy difference between occupied and unoccupied states. Because in second-order perturbation theory the MAE is inversely proportional to the energy separation between occupied and unoccupied states, a strong MAE is predicted and experimentally observed for the c/a ratio minimizing this energy separation.[5,7]

This picture changes completely when considering a single Fe_xCo_{1-x} layer on the Pt(111) surface. In this case, the c/a ratio is not even defined. The symmetry breaking arises from coordination reduction, strain due to lattice mismatch between monolayer and substrate, and electronic hybridization with the substrate. The calculations evidence a charge transfer from the Pt substrate to the Fe_xCo_{1-x} film, changing more or less linearly from about 0.08 electrons for pure Co to 0.06 electrons for pure Fe. The effect of the electronic hybridization with the substrate can be qualitatively understood by comparing each of the five orbital-resolved DOS calculated for the Co/Pt(111) monolayer film (Fig. 12) with the equivalent calculated for the free-standing Co monolayer (see Fig. 2 of Ref. 66). The most visible difference concerns the DOS widths of the two systems. For $m_l=\pm2$ the DOS

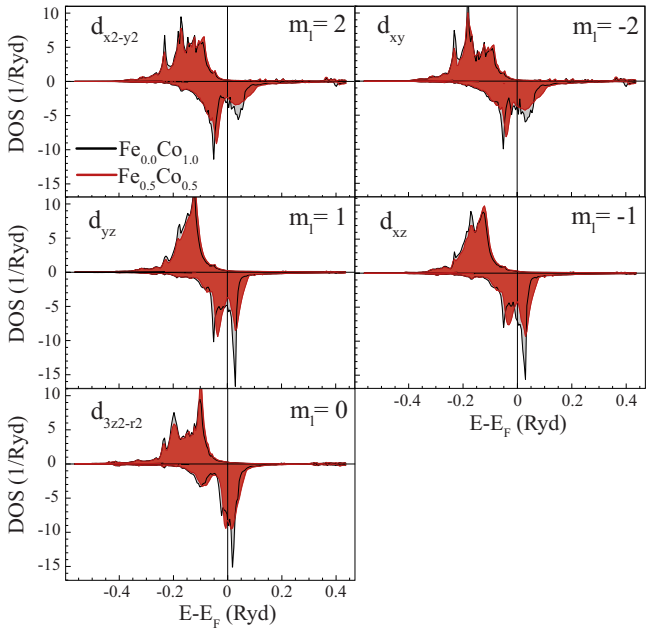

FIG. 12. (Color online) Orbital-resolved Co DOS calculated for $Fe_{0.5}Co_{0.5}$ and for the pure Co monolayer films.

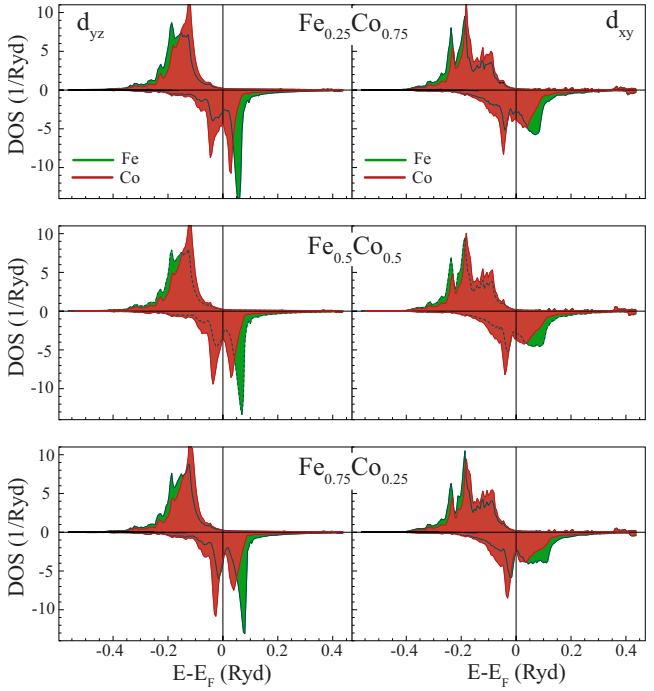

FIG. 13. (Color online) Orbital-resolved DOS for Fe and Co as a function of the alloy stoichiometry. Reducing the Co content produces for both elements the broadening of in-plane (d_{xy}) and out-of-plane (d_{yz}) orbitals. A similar trend is also observed for the other d orbitals.

widths are very similar, while for $m_l=\pm 1$ and $m_l=0$ the DOS widths are about 3 and 4 eV, respectively, larger in the Pt(111) supported Co monolayer. In the independent electron ligand field picture a larger DOS width implies stronger electronic hybridization or bonding with the neighboring atoms.[67] Because orbitals with $m_l=0$ $(d_{3z^2-r^2})$ and $m_l=\pm 1$ (d_{xz},d_{yz}) describe out-of-plane bonding, while orbitals with $m_l=\pm 2$ $(d_{x^2-y^2},d_{xy})$ describe in-plane bonding, the previous observation on the DOS widths immediately highlights the formation of a strong vertical Co-Pt bonding and a substantially unmodified in-plane Co-Co bonding. In the same ligand field picture, the formation of a strong directional bonding generates a reduction in the component of the orbital moment perpendicular to the bonding direction. In our case, this implies a strong reduction in the in-plane component of the orbital moment in the Co/Pt(111) monolayer in comparison with the free-standing monolayer. Coherently, our experimental data show highly unquenched out-of-plane orbital atomic moments of $L=(0.31\pm 0.06)\mu_B$ and $(0.14\pm 0.02)\mu_B$ for pure Co and Fe, respectively.

A second strong hybridization is seen between Fe and Co atoms when they are mixed in the alloy. Because the Co DOS is narrower than the Fe DOS, increasing the Fe percentage in the alloy leads to the spreading of Co and Fe DOS (Fig. 13). However, the orbital-resolved DOS for Co are always narrower than the corresponding one for Fe. In the ligand field picture this implies larger L values for Co than for Fe, in agreement with the experiment.

The Fe-Co hybridization is also responsible for the observed composition dependence of the MAE. To highlight this point, we compared the anisotropy of the orbital moment $(\Delta L=L_{M\perp}-L_{M\parallel})$ with the anisotropy in the occupation of each minority $3d\downarrow$ orbitals $(\Delta N_d\downarrow=N_{d,M\parallel}-N_{d,M\perp})$ calculated for the magnetization oriented out of plane $(M\perp)$ and in plane $(M\parallel)$ (Fig. 14). In order to simplify the comparison we weighted the differences in the occupation of the minority $3d\downarrow$ orbitals with the corresponding orbital quantum numbers. This way, for the $d_{x^2-y^2}$ and d_{xy} in-plane orbitals the anisotropy reads $\Delta N_{\mathrm{ip}}\downarrow=2(\Delta N_{xy}-\Delta N_{x^2-y^2})$ while for the d_{xz} and d_{yz} out-of-plane orbitals reads $\Delta N_{\mathrm{op}}\downarrow=\Delta N_{xz}-\Delta N_{yz}$. The $d_{3z^2-r^2}$ $(m_l=0)$ out-of-plane orbital gives no contribution to the orbital moment and was therefore left out. Because the majority states give only a minor contribution, this allows direct linking of the occupation number with the orbital moment. We also note that the pure d orbitals have $m_l=0$. However, the spin-orbit interaction produces a mixing of the d orbitals which lifts the m_l degeneracy. The resulting curves clearly suggest that the maximum of the orbital moment anisotropy occurs at equiatomic composition as a result of the occupation change in the $d_{x^2-y^2}$ and d_{xy} orbitals, both for Fe and Co, while the in-plane orbitals give an almost composition independent contribution. Because in the Bruno[68] and van der Laan[69] models the MAE is directly linked to ΔL, we can argue that also the maximum MAE observed for the same composition is a strict consequence of this fine tuning of the occupation in the $3d\downarrow$ orbitals.

As a final remark we want to stress the relevant role played by the substrate. The Pt surface, transferring charge and forcing a morphological strain in the overlayer FeCo film, completely modifies the film electronic structure. This means that the system has to be described as a whole and trying to extrapolate general trends could be misleading. In the previous discussion, when attributing to the Fe-Co hybridization the bell shape of the MAE vs stoichiometry curve, we intended to highlight that the major effect of the

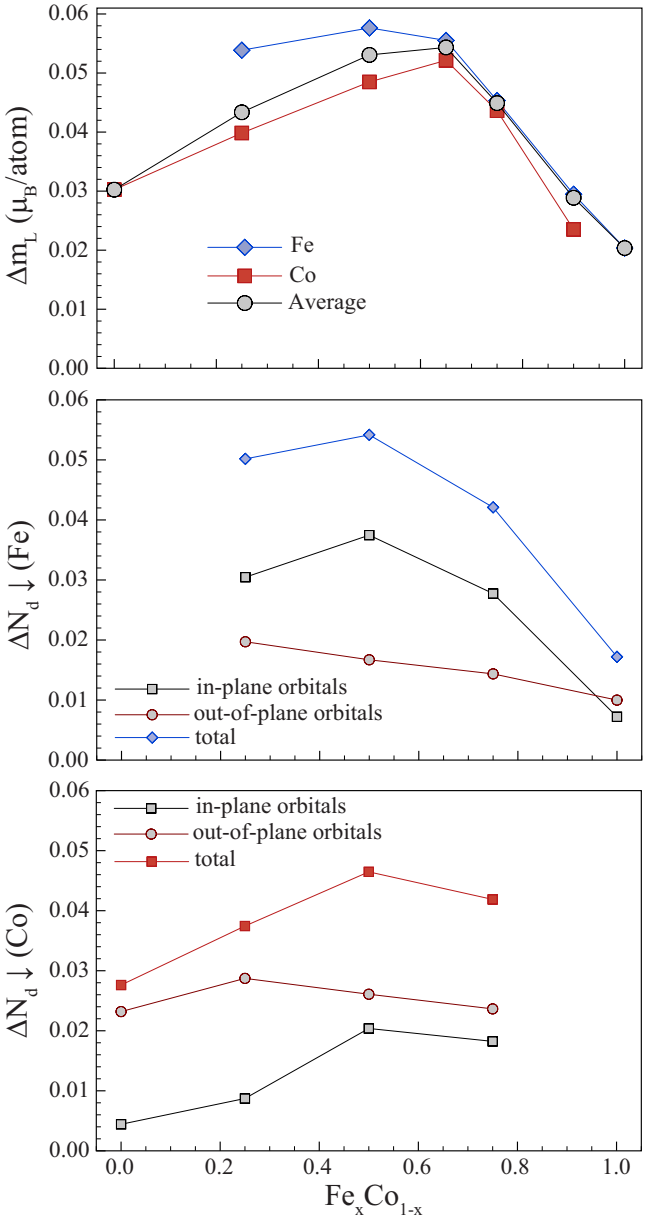

FIG. 14. (Color online) Anisotropy of orbital moments (top) compared to the anisotropy of the occupation of spin-down orbitals of Fe (middle) and Co (bottom). Lines are guides for the eyes.

electronic hybridization involving Fe, Co, and Pt atoms is seen in the in-plane *d* orbitals of Fe and Co even if the Pt plays a non-negligible role. This is clearly seen comparing, for example, our results with similar ones for an FeCo monolayer on Cu(100).[70] In this last case the MAE is found to have a linear dependence on the film composition.

VI. CONCLUSIONS

The magnetic moments, magnetic anisotropy energies, and coercive fields of monolayer-thick granular and continuous Fe_xCo_{1-x} films deposited on a Pt(111) surface have been investigated by XMCD and MOKE, as well as by first-principles electronic structure calculations. XMCD data show that the effective spin moment of Co and Fe is not correlated with the stoichiometry in granular films, contrary to the orbital moment, which shows a maximum at $x=0.35$ for both Fe and Co. The calculated atomic spin moments of Fe and Co are close to $3.0\mu_B$ and $2.0\mu_B$, respectively, and only weakly composition dependent. The calculated orbital moments of Fe and Co are shown to depend on the stoichiometry, with a maximum around $x=0.6$ for both species. The total (spin plus orbital) magnetic moment of the alloyed film does not follow the well-known bell-shaped Slater-Pauling curve[15] observed in bulk bcc FeCo alloys due to the monotonic linear dependence of the average spin moment on the film composition. The calculated DOS shows that this behavior is due to the reduced film dimensionality which, narrowing the *d*-DOS, produces a clear splitting of the Fe $3d\uparrow$ and $3d\downarrow$ spin bands. The MAE strongly depends on the alloy composition and follows the orbital moment trend, with a maximum around $x=0.4$ (experiment) and $x=0.6$ (theory). The largest MAE value is 0.5 meV/atom, which is more than 2 orders of magnitude greater than the MAE of bcc FeCo alloys and similar to the MAE of the highly ordered $L1_0$ phase of FePt. The element and orbital-resolved DOS clearly demonstrate that the observed composition dependence is the result of fine changes of the relative population of spin-down $d_{x^2-y^2}$ and d_{xy} in-plane orbitals, both for Fe and Co, while the $d_{3z^2-r^2}$, d_{xz}, and d_{yz} out-of-plane orbitals play no role. Charge transfer from the Pt substrate to the overlayer film, together with spin and orbital moments induced in the Pt atoms, are found to affect both the Fe-Co hybridization and the overall magnetic properties.

ACKNOWLEDGMENTS

One of us (J.Z.) would like to thank R. Hammerling and P. Mohn for helpful discussions. Financial support from the Swiss National Science Foundation (Grants No. 200020-109800 and No. 200020-112322) and from the Austrian Science Fund (FWF) within the Joint Research Programme S90 are gratefully acknowledged. Financial support of this work was also provided by the Austrian Science Foundation (Grant No. WK W004) and Oak Ridge National Laboratory (Subcontracts No. 4000043271 and No. 4000063148). We acknowledge the ESRF for provision of beam time and financial support from the EUROCORES 05-SONS-FP-009 SANMAG project of the European Science Foundation.

[1] *The Physics of Ultra-High-Density Magnetic Recording*, Springer Series in Surface Sciences Vol. 41, edited by M. L. Plumer, J. van Ek, and D. Weller (Springer, Berlin, 2001).
[2] B. M. Lairson and B. M. Clemens, Appl. Phys. Lett. **63**, 1438 (1993).
[3] C. Antoniak *et al.*, Phys. Rev. Lett. **97**, 117201 (2006).
[4] S. Sun, C. B. Murray, D. Weller, L. Folks, and A. Moser, Science **287**, 1989 (2000).
[5] T. Burkert, L. Nordstrom, O. Eriksson, and O. Heinonen, Phys. Rev. Lett. **93**, 027203 (2004).
[6] A. Winkelmann, M. Przybylski, F. Luo, Y. Shi, and J. Barthel, Phys. Rev. Lett. **96**, 257205 (2006).
[7] F. Yildiz, F. Luo, C. Tieg, R. M. Abrudan, X. L. Fu, A. Winkelmann, M. Przybylski, and J. Kirschner, Phys. Rev. Lett. **100**, 037205 (2008).
[8] P. Gambardella *et al.*, Science **300**, 1130 (2003).
[9] P. Gambardella, S. S. Dhesi, S. Gardonio, C. Grazioli, P. Ohresser, and C. Carbone, Phys. Rev. Lett. **88**, 047202 (2002).
[10] D. Sander, S. Ouazi, A. Enders, T. Gutjahr-Löser, V. S. Stepanyuk, D. I. Bazhanov, and J. Kirschner, J. Phys.: Condens. Matter **14**, 4165 (2002).
[11] C. J. Lin, G. L. Gorman, C. H. Lee, R. F. C. Farrow, E. E. Marinero, H. V. Do, H. Notarys, and C. J. Chien, J. Magn. Magn. Mater. **93**, 194 (1991).
[12] N. W. E. McGee, M. T. Johnson, J. J. de Vries, and J. aan de Stegge, J. Appl. Phys. **73**, 3418 (1993).
[13] T. Katayama, Y. Suzuki, Y. Nishihara, T. Sugimoto, and M. Hashimoto, J. Appl. Phys. **69**, 5658 (1991).
[14] D. Weller and A. Moser, IEEE Trans. Magn. **35**, 4423 (1999).
[15] L. Pauling, Phys. Rev. **54**, 899 (1938).
[16] R. C. Hall, J. Appl. Phys. **31**, S157 (1960).
[17] K. Inomata, T. Sawa, and S. Hashimoto, J. Appl. Phys. **64**, 2537 (1988).
[18] H. Brune, Surf. Sci. Rep. **31**, 121 (1998).
[19] K. Bromann, H. Brune, M. Giovannini, and K. Kern, Surf. Sci. **388**, L1107 (1997).
[20] T. Cren, S. Rusponi, N. Weiss, M. Epple, and H. Brune, J. Phys. Chem. B **108**, 14685 (2004).
[21] D. Repetto *et al.*, Phys. Rev. B **74**, 054408 (2006).
[22] E. Lundgren, B. Stanka, M. Schmid, and P. Varga, Phys. Rev. B **62**, 2843 (2000).
[23] P. Bruno, G. Bayreuther, P. Beauvillain, and C. Chappert, J. Appl. Phys. **68**, 5759 (1990).
[24] M. Przybylski, L. Yan, J. Zukrowski, M. Nyvlt, Y. Shi, A. Winkelmann, J. Barthel, M. Wasniowska, and J. Kirschner, Phys. Rev. B **73**, 085413 (2006).
[25] S. Ferrer, J. Alvarez, E. Lundgren, X. Torrelles, P. Fajardo, and F. Boscherini, Phys. Rev. B **56**, 9848 (1997).
[26] O. Robach, C. Quiros, P. Steadman, K. F. Peters, E. Lundgren, J. Alvarez, H. Isern, and S. Ferrer, Phys. Rev. B **65**, 054423 (2002).
[27] H. Bulou and C. Massobrio, Phys. Rev. B **72**, 205427 (2005).
[28] Y. Xie and J. A. Blackman, Phys. Rev. B **74**, 054401 (2006).
[29] B. T. Thole, P. Carra, F. Sette, and G. van der Laan, Phys. Rev. Lett. **68**, 1943 (1992).
[30] P. Carra, B. T. Thole, M. Altarelli, and X. Wang, Phys. Rev. Lett. **70**, 694 (1993).
[31] C. T. Chen, Y. U. Idzerda, H. J. Lin, N. V. Smith, G. Meigs, E. Chaban, G. H. Ho, E. Pellegrin, and F. Sette, Phys. Rev. Lett. **75**, 152 (1995).
[32] H. H. Hamdeh, B. Fultz, and D. H. Pearson, Phys. Rev. B **39**, 11233 (1989).
[33] R. Wu and A. J. Freeman, Phys. Rev. Lett. **73**, 1994 (1994).
[34] J. G. Amar, F. Family, and P.-M. Lam, Phys. Rev. B **50**, 8781 (1994).
[35] R. Skomski, H.-P. Oepen, and J. Kirschner, Phys. Rev. B **58**, 3223 (1998).
[36] A. Vaterlaus, O. Portmann, C. Stamm, and D. Pescia, J. Magn. Magn. Mater. **272-276**, 1137 (2004).
[37] R. M. Bozorth, Phys. Rev. **50**, 1076 (1936).
[38] P. Gambardella, A. Dallmeyer, K. Maiti, M. C. Malagoli, S. Rusponi, P. Ohresser, W. Eberhardt, C. Carbone, and K. Kern, Phys. Rev. Lett. **93**, 077203 (2004).
[39] R. Wu, L. Chen, and N. Kioussis, J. Appl. Phys. **79**, 4783 (1996).
[40] A. Arrott, Phys. Rev. **108**, 1394 (1957).
[41] J. S. Kouvel, General Electric Research Laboratory Report No. 57-RL-1799 (1957).
[42] P. Poulopoulos, M. Farle, U. Bovensiepen, and K. Baberschke, Phys. Rev. B **55**, R11961 (1997).
[43] R. Skomski, J. Phys.: Condens. Matter **15**, R841 (2003).
[44] C. Takahashi, M. Ogura, and H. Akai, J. Phys.: Condens. Matter **19**, 365233 (2007).
[45] M. Lezaic, P. Mavropoulos, and S. Bluegel, Appl. Phys. Lett. **90**, 082504 (2007).
[46] M. Pratzer and H. J. Elmers, Phys. Rev. Lett. **90**, 077201 (2003).
[47] D. Spišák and J. Hafner, Phys. Rev. B **70**, 014430 (2004).
[48] L. Szunyogh, B. Újfalussy, P. Weinberger, and J. Kollár, Phys. Rev. B **49**, 2721 (1994).
[49] H. J. F. Jansen, Phys. Rev. B **59**, 4699 (1999).
[50] *Electron Scattering in Solid Matter*, edited by J. Zabloudil, R. Hammerling, L. Szunyogh, and P. Weinberger (Springer-Verlag, Heidelberg, 2004).
[51] I. Turek, J. Kudrnovsky, V. Drchal, and P. Weinberger, Phys. Rev. B **49**, 3352 (1994).
[52] G. Andersson, T. Burkert, P. Warnicke, M. Björck, B. Sanyal, C. Chacon, C. Zlotea, L. Nordström, P. Nordblad, and O. Eriksson, Phys. Rev. Lett. **96**, 037205 (2006).
[53] A. Kleibert, J. Passig, K.-H. Meiwes-Broer, M. Getzlaff, and J. Bansmann, J. Appl. Phys. **101**, 114318 (2007).
[54] S. Imada, A. Yamasaki, S. Suga, T. Shima, and K. Takanashi, Appl. Phys. Lett. **90**, 132507 (2007).
[55] O. Dmitrieva *et al.*, Phys. Rev. B **76**, 064414 (2007).
[56] W. J. Antel, Jr., M. M. Schwickert, T. Lin, W. L. O'Brien, and G. R. Harp, Phys. Rev. B **60**, 12933 (1999).
[57] P. Ohresser, G. Ghiringhelli, O. Tjernberg, N. B. Brookes, and M. Finazzi, Phys. Rev. B **62**, 5803 (2000).
[58] M. A. Torija, Z. Gai, N. Myoung, E. W. Plummer, and J. Shen, Phys. Rev. Lett. **95**, 027201 (2005).
[59] P. Ohresser, N. B. Brookes, S. Padovani, F. Scheurer, and H. Bulou, Phys. Rev. B **64**, 104429 (2001).
[60] K. von Bergmann, S. Heinze, M. Bode, E. Y. Vedmedenko, G. Bihlmayer, S. Blügel, and R. Wiesendanger, Phys. Rev. Lett. **96**, 167203 (2006).
[61] I. Yang, S. Y. Savrasov, and G. Kotliar, Phys. Rev. Lett. **87**, 216405 (2001).
[62] *Physics of Ferromagnetism*, edited by S. Chikazumi (Clarendon, Oxford, 1997).
[63] R. Richter and H. Eschrig, J. Phys. F: Met. Phys. **18**, 1813 (1988).

[64] R. H. Victora and L. M. Falicov, Phys. Rev. B **30**, 259 (1984).
[65] R. H. Victora, L. M. Falicov, and S. Ishida, Phys. Rev. B **30**, 3896 (1984).
[66] G. H. O. Daalderop, P. J. Kelly, and M. F. H. Schuurmans, Phys. Rev. B **50**, 9989 (1994).
[67] J. Stöhr, J. Magn. Magn. Mater. **200**, 470 (1999).
[68] P. Bruno, Phys. Rev. B **39**, 865 (1989).
[69] G. van der Laan, J. Phys.: Condens. Matter **10**, 3239 (1998).
[70] C. Etz, B. Lazarovits, J. Zabloudil, R. Hammerling, B. Újfalussy, L. Szunyogh, G. M. Stocks, and P. Weinberger, Phys. Rev. B **75**, 245432 (2007).